J Mater Sci: Mater Electron (2025) 36:345

Optical transmittance, optical homogeneity, HRXRD and third-order NLO properties of an organic 1H-benzotriazole salicylic acid (BHSA) single crystals

T. Kamalesh[1], P. Karuppasamy[2], Muthu Senthil Pandian[2], G. Durgababu[3], V. Mohankumar[4], V. Kayalvizhi[5], Mohd Afzal[6], and RO. MU. Jauhar[5,*]

[1] *Department of Physics, B. S. Abdur Rahman Crescent Institute of Science and Technology, Chennai 600 048, India*
[2] *SSN Research Centre, Sri Sivasubramaniya Nadar College of Engineering, Kalavakkam 603110, India*
[3] *Department of Physics, Rajiv Gandhi University of Knowledge Technologies, Nuzvid, AndhraPradesh 521 202, India*
[4] *Department of Physics, PSG College of Arts and Science, Coimbatore 641014, India*
[5] *Department of Physics, Saveetha School of Engineering, SIMATS, Chennai 602105, India*
[6] *Department of Chemistry, College of Science, King Saud University, 11451 Riyadh, Saudi Arabia*

Received: 16 December 2024
Accepted: 8 February 2025

ABSTRACT

The single crystals of an organic 1H-benzotriazole salicylic acid (BHSA) were harvested adopting solution growth method (SEST) and the characterizations carried out in the subsequent sections emphasize that it is reported for the first time in the literature with regards to the title crystal. The structural parameters of the grown crystals were assessed using XRD technique. The presence of internal structural grain boundaries was analyzed using high-resolution XRD (HRXRD) along (1 0 -1) plane. The vibrational assignments in the material were assessed using Fourier transform infrared (FTIR) analysis. The optical transmittance is found to be 67% with its cut-off and bandgap to be 339 nm and 3.55 eV, respectively. The stability as assessed by TGA-DTA is found to be 131 °C. The density of etch pits were 57.6×10^3 cm^{-2} for 4 s, 40×10^3 cm^{-2} for 6 s. Optical homogeneity has been analysed from birefringence interferometry. Brewster's angle method was adopted to find the refractive index of the title material. Z-scan technique revealed the third-order nonlinear optical properties of the BHSA crystal.

1 Introduction

All these years, crystal growth has gained prominence as a subject of study that crosses several disciplines, including chemistry, engineering, physics, and materials science. For a range of uses in laser technology, image processing, optical computing, optoelectric switching, and data storage devices, nonlinear optical (NLO) materials have been developed [1–4]. Growing organic single crystals piqued

Address correspondence to E-mail: jauharphysicist@gmail.com

https://doi.org/10.1007/s10854-025-14415-9
Published online: 19 February 2025

the interest of crystal researchers as they are cost effective, enhance significant hyperpolarizability (β) and higher LDT values. However, organic crystals have weaker mechanical and thermal characteristics than their inorganic counterparts [5]. Nonlinearity in organic material is typically caused by the existence of delocalised π-electron attaching donor and acceptor groups [5]. Because triazole compounds have several uses in both business and agriculture, researchers have been synthesising them over the past few decades [6]. The empirical formula for benzotriazole, also known as 1H-benzotriazole, is $C_6H_5N_3$. It is a heterocyclic molecule. The nitrogen (N) covered bicyclic ring structure known as the benzotriazole family has been known to have wide range of biological benefits, including anti-inflammatory, analgesic, antimalarial, and antitubercular activity [6–8]. The combination of hydrogen-bonding/donating sites, 1H-benzotriazole and salicylic acid (carboxylic acid) are synthesized in view of a variety of research prospects for binary compounds [7]. It has been observed that there is no change in connection when the self-complementary component is incorporated into the structure. The structure of the title compound was reported by Wang Lei et al. [7]. In the present research, solvent evaporation method (SESM) was adopted to develop the organic 1H-benzotriazole and salicylic acid (BHSA) single crystal. Salicylic acid and the 1H-benzotriazole molecule form acid–base type cocrystals, which serve as the foundation for the BHSA single crystal. The strong hydrogen interactions (N–H–O, O–H–N and O–H–O) and weak C–H–O interactions built by cocrystals through H-bonding are essential in the growth of BHSA single crystals [7].

The BHSA grown crystal has been characterized by morphology, Solubility, Single crystal XRD, Powder XRD, HRXRD, FTIR, optical transmittance study, TG/DTA, chemical etching studies, birefringence interferometry technique, Brewster's angle method and Z-scan technique.

2 Experimental procedure

2.1 Material synthesis

The 1H-benzotriazole and salicylic acid were taken in a 1:1 equimolar ratio using methanol as solvent. The calculated quantity of 1H-Benzotriazole (8.624 g) was dissolved in methanol solvent (200 ml beaker) at room temperature, then salicylic acid (10 g) was gradually added to the solution containing 1H-Benzotriazole. As homogenization of the solution is important in the growth aspect the solution was stirred for 12 h continuously. Then the solution was filtered and transferred to the petri dish for crystallization at room temperature. The petri dish was covered with perforated thick plastic cover to control evaporation. After 28 days, BHSA single crystals with dimensions of 10 mm × 5 mm × 2 mm were harvested. Figure 1a reveals the as grown BHSA single crystals. Figure 1b shows the morphology of the BHSA crystal.

2.2 Solubility

In the solution growth method, the selection of a solvent (water, methanol, acetone, etc.,) plays a major role. Solubility is defined as the amount of solute dissolved in the solvent at a given temperature. Solubility is one of the most vital factors in growing large size single crystals by slow cooling, seed rotation, Sankaranarayana-Ramasamy and Immersed ampoule Sankaranarayana-Ramasamy method. According to a pharmaceutical point of view, the dissolvability of a drug plays a significant part to enhance the drug

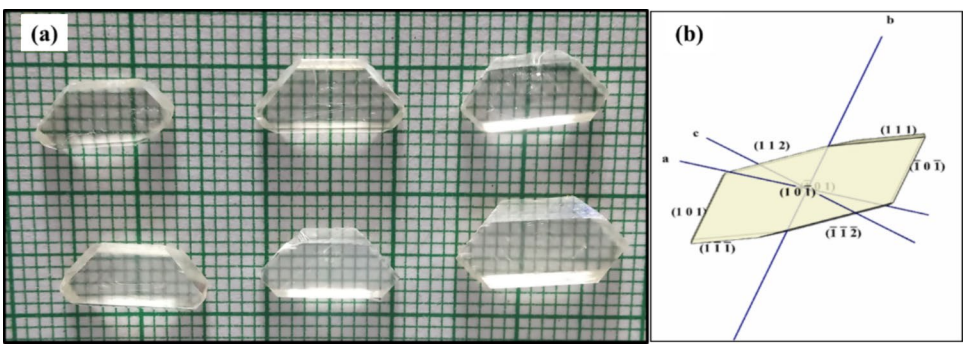

Fig. 1 **a** As grown BHSA single crystals and (**b**) its Morphology

bioavailability [9–11]. Different crystal has different lattice energies and enthalpies, hence the solubility is also different [12]. The solubility of BHSA was carried out using the constant temperature bath (CTB) at different temperatures from 30 °C to 60 °C. Initially, the CTB (accuracy ± 0.01 ºC) was controlled at 30 ºC. 100 ml of methanol was taken in a conical flask with continuous stirring. The BHSA (powder material) was added slowly into a conical flask. After a point to confirm the saturation little more amount of the powdered material was added to the solution hence to calculate the equilibrium concentration of the solute gravimetrically. The same process was followed for various concentrations ranging from 35˚C- 60˚C at 5˚ interval. The solubility curve of BHSA is shown Fig. 2. The solubility spectrum reveals that BHSA single crystal has positive solubility gradient in the methanol solvent. This can be due to the fact that the BHSA undergoes endothermic reaction. Table 1 shows the Solubility data of BHSA single crystal dissolved in methanol solvent at different temperatures.

3 Results and discussion

3.1 X-ray diffraction (XRD) studies

The space group and other structural-related parameters of the BHSA single crystal as assessed from single crystal XRD reveals that it falls under monoclinic crystal system with $P2_1/n$ space group. The values attained are $a = 13.819$ (2) Å, $b = 5.392$ (8) Å, $c = 16.710$ (3) Å, $\alpha = 90º$, $\beta = 102.34º$, $\gamma = 90º$ with volume (V) to be 1216.4 $Å^3$ and these values are in good agreement with the literature [7] that is given in Table 2. The Powder XRD spectrum of BHSA was determined using PANalytical X-ray diffractometer ($\lambda = 1.5406$ Å) at room temperature and it agrees well with CIF data. The comparative spectrum between the experimental and theoretical points are shown in Fig. 3. The sharp peak indicates the precise quality of the grown BHSA crystal.

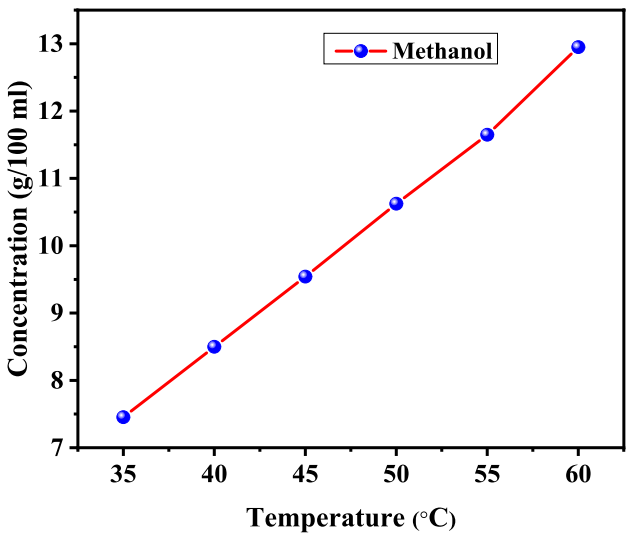

Fig. 2 Solubility curve of BHSA crystal

Table 1 The Solubility of BHSA single crystal at different temperatures

S.No	Temperature (˚C)	Concentration (g/100 ml)
1	35 (room temperature)	7.5
2	40	8.5
3	45	9.5
4	50	10.6
5	55	11.7
6	60	13

3.2 High-Resolution XRD (HRXRD) analysis

The crystalline perfection and internal structural grain boundaries of the BHSA have been analyzed by PANalytical Empyrean HRXRD measurement [2]. Figure 4 reveals the PXRD spectrum taken along (1 0 -1) direction of BHSA single crystal. The obtained peaks indicate (1 0 -1) family planes while the (1 0 -1) and (2 0 -2) planes were used for HRXRD measurement as shown in Fig. 5 with the Bragg angle (2θ) to be 7.5˚ and 15.1˚, respectively. The HRXRD spectra

Table 2 Lattice parameters of BHSA single crystal

Lattice parameters	Wang, Lei et al. [7]	Present Work
a (Å)	13.786 (5)	13.819
b (Å)	5.372 (2)	5.3922
c (Å)	16.688 (6)	16.710
A	90.0˚	90.0˚
B	101.905 (6) ˚	102.344˚
Γ	90.0˚	90.0˚
V($Å^3$)	1209 (7)	1216.4
System	Monoclinic	Monoclinic
Space group	$P2_1/n$	$P2_1/n$

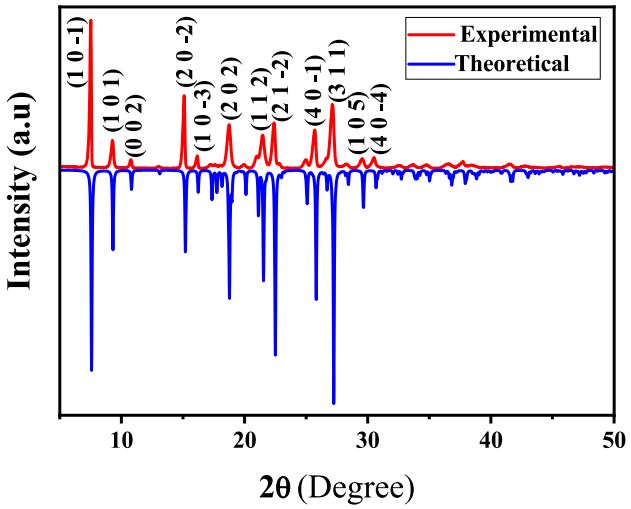

Fig. 3 Powder XRD pattern of BHSA single crystal

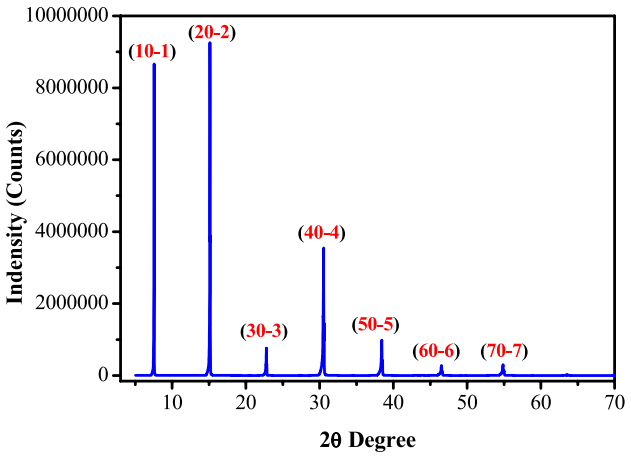

Fig. 4 XRD spectrum along < 1 0 -1 > direction of BHSA single crystal

show that the appeared diffraction curve (DC) on (1 0 -1) and (2 0 -2) planes are single peaks as any additional peaks at the corresponding 2θ positions are not spotted. This indicates that the BHSA single crystal is free from structural grain boundaries [13]. The full width at half maximum (FWHM) of the peaks on (1 0 -1) and (2 0 -2) are 51.4" and 52.6", respectively. The broadening of rocking curve without the presence of any splitting and without much asymmetry with respect to the peak position can be attributed to defects like randomly oriented mosaic blocks, dislocations, Frankel defects. Cracks and structural grain boundaries result from defects that are not statistically distributed but rather dispersed as macroscopic clusters. These clusters produce greater strain, which is seen in HRXRD curves as an extra peak or peak(s). On the other hand, a vacancy defect may be the cause of the significant bulging towards the left of the DC. However, the BHSA crystal exhibits good crystalline perfection as evidenced by the sharp DC and lack of extra peaks [13, 14].

3.3 FTIR analysis

Bruker AXS FTIR spectrometer was utilized to record the FTIR spectrum in the prescribed range as shown in Fig. 6. The vibrational assignments related to the wavenumbers are listed in Table 3 [7, 15].

3.4 Optical transmittance study

Optical transmittance is used to analyze the number of conjugations of the double bond and aromatic conjugation within the molecule. It relates the elevation of electrons from HOMO to LUMO [9, 16]. The Shimadzu UV-2600i double-beam spectrophotometer was utilized to record the optical transmission spectrum of BHSA crystal in the range between 200 and 900 nm as shown in Fig. 7. The BHSA crystal (2 mm thickness) has 67% optical transmittance in the entire visible region with lower cut-off wavelength to be 339 nm. From these observations it is found that the grown BHSA crystal has good optical transparency in the entire visible region making it suitable for optical limiting applications.

The optical properties like absorption coefficient (α) and other parameters were calculated using standard expressions [2, 17, 18].

The optical band gap (E_g) was calculated from Tauc's plot relation by extrapolating the linear part of the y-axis to the energy axis as shown in Fig. 8a [19–21]. The bandgap obtained through Tauc's plot is found to be 3.55 eV. The spectrum for Extinction coefficient (K), Reflectance (R) and Refractive index (n_o) shown in Fig. 8b, c & d were calculated using standard expressions [17].

shows the extinction coefficient (K), reflectance (R) and refractive index (n_o) spectra of the BHSA crystal.

3.5 Thermal analysis

TGA/DTA was carried out in the range between 30°C and 350 °C to find the thermal stability and phase transitions involved in the BHSA crystal as

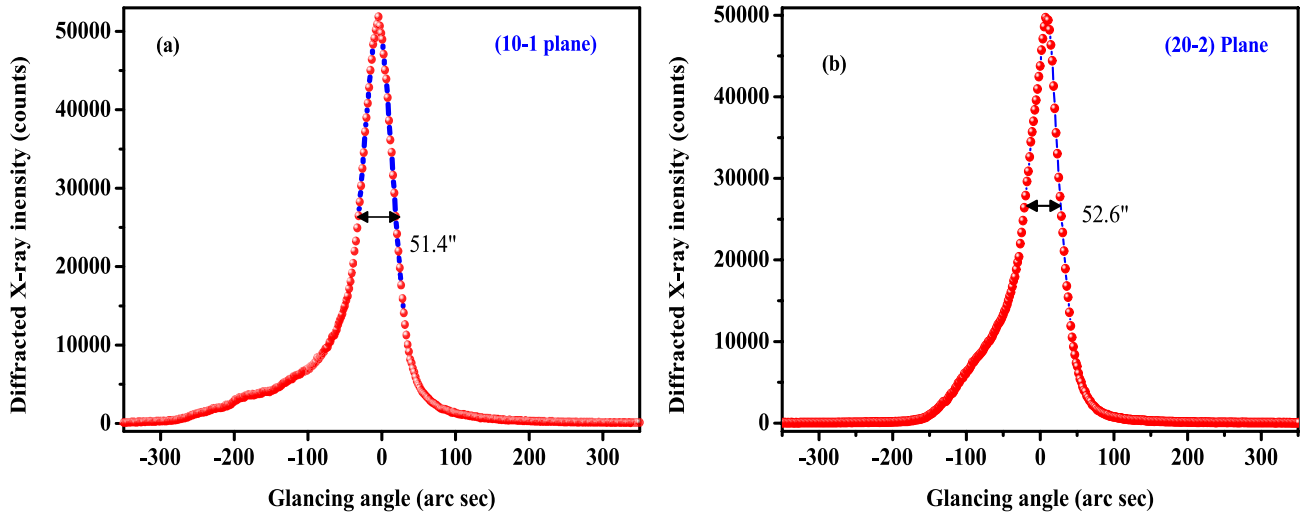

Fig. 5 HRXRD spectra of (1 0 -1) and (2 0 -2) planes BHSA single crystal

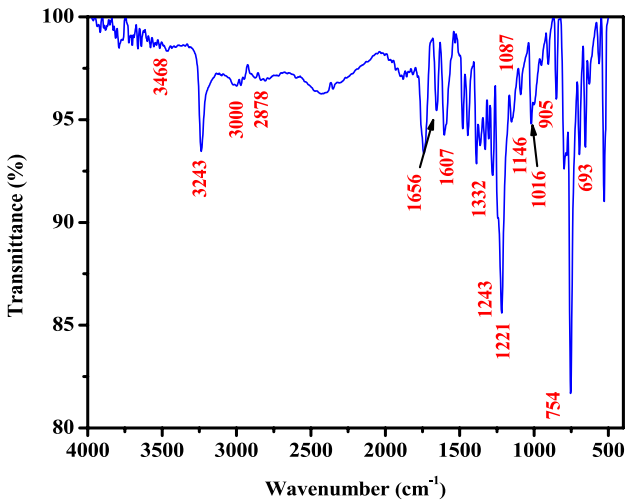

Fig. 6 FTIR spectrum of BHSA

shown in Fig. 9. From the TGA curve it is observed that the BHSA is stable upto 130 °C. The first stage weight loss pattern with respect to the corresponding endothermic peak in the DTA curve upholds the fact that the material starts to decompose from 131 °C till 139 °C.

Further the second stage and third stage weight loss ranges from 150 °C to 226 °C with the removal of material into gaseous products (mixture of CO, CO_2, NO, and hydrocarbons), and decomposition process was further continued till 350 °C. From these observations one can conclude that the BHSA crystal may be utilized for any applications below 130 °C.

3.6 Chemical etching analysis

Good quality BHSA crystal was used for etching analysis along < 10–1 > plane employing COSLAB (Model CMM-23) optical microscope with ethylene glycol as etchant. The BHSA crystal surface (10–1) was immersed in ethylene glycol and the crystal surface has been observed through optical microscope. The etching time was increased from 2 to 10 s with an interval of 2 s and the corresponding rectangular-shaped etch pit patterns were captured through a optical microscope. The crystal surface before and after etching are shown in Fig. 10a-f. From the figure it is observed that on increasing the etching time enlarged etch pits were observed rather disappear but to be precise with etching time of 10 s and above the etch pits were found to overlap and disappear. The following expression [22–25] was used to calculate the etch pit density (EPD)

$$\text{EPD} = \frac{\text{Number of etch pits}}{\text{Area}} \quad (1)$$

The EPD values of the BHSA crystal (10–1) were 57.6×10^3 cm^{-2} for 4 s, 40×10^3 cm^{-2} for 6 s, 12.8×10^3 cm^{-2} for 8 s and 3.6×10^3 cm^{-2} for 10 s. The observed values are found to be low indicating the atoms/molecules are packed systematically during the growth [23].

Table 3 Peak assessment of BHSA crystal

Wave number (cm^{-1})	Mode of vibrations	Assignments [7, 15]
3468	O–H stretching	hydrogen-bonded presence of COOH-group
3243	O–H stretching	Presence of OH-group
1656	O–H stretching	Presence of COOH-group
1243	O–H in plane bending	Presence of COOH-group
1146	C-O stretching	Presence of COOH-group
905	O–H out of plane bending	Presence of COOH-group
1221	C-O stretching	Presence of phenolic group
1332	O–H in plane bending	Presence of phenolic group
693	O–H out of plane bending	Presence of phenolic group
3000 & 3100	aromatic C-H stretching	Presence of aromatic ring
1607	C = C stretching	Presence of aromatic ring
1016 & 1087	C-H in of plane bending	Presence of aromatic ring
754	C-H out of plane bending	Presence of 1, 4 disubstituted benzene ring
2878	N–H stretching	Presence of N–H group

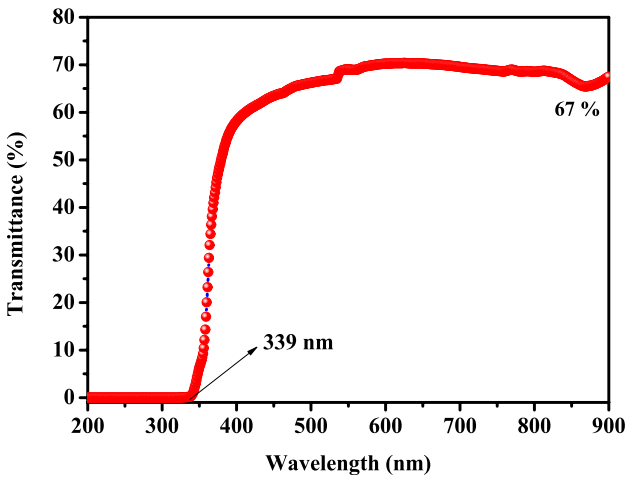

Fig. 7 UV–Vis NIR spectrum of BHSA single crystal

3.7 Birefringence studies

The birefringence measurement was carried out on the BHSA crystal to reveal its optical homogeneity. The polished BHSA crystal (1 mm and along < 101 > direction) was subjected to a birefringence interferometer. In general, there are two ways to analyse Birefringence interferometry: (i) conoscopy, which analyses the beam in a converged state, and (ii) orthoscopy, which analyses the beam in a parallel state [29]. The shape of the resulting fringes could be used to evaluate the homogeneity in the refractive index. The birefringence interferogram of the BHSA crystal is displayed in Fig. 11. The image illustrates that the fringes are parallel and well-spaced, indicating that the optical homogeneity of the grown crystal is good. One possible explanation for the equidistant fringes' and parallel spacing is due to the wedge present in the sample [26, 27].

3.8 Refractive index

The Brewster's angle method was utilized to determine the refractive index of the material. A diode laser (650 nm) was used as the light source, which was directed onto the surface of the BHSA crystal through a polarizer. The reflected beam from the sample was then collected by the detector [27]. The sample was rotated along (15°, 20°, 25° …0.70°) and the corresponding reflected beam was noted. From these observations the refractive index of the grown BHSA crystal was found to be 1.6. The angle of rotation versus detector output is shown in Fig. 12.

Generally, at a particular point the output intensity is found to be minimum and is said to be the Brewster's angle or polarizing angle (i_p or θ_p). The refractive index of the BHSA crystal was calculated following expression [27–29].

$$\mu = \tan i_p \tag{2}$$

where i_p and μ are Brewster's angle or polarizing angle of the sample (from the graph 58.1°) and the refractive index of the sample, respectively. The refractive index of the BHSA crystal is 1.6 (650 nm).

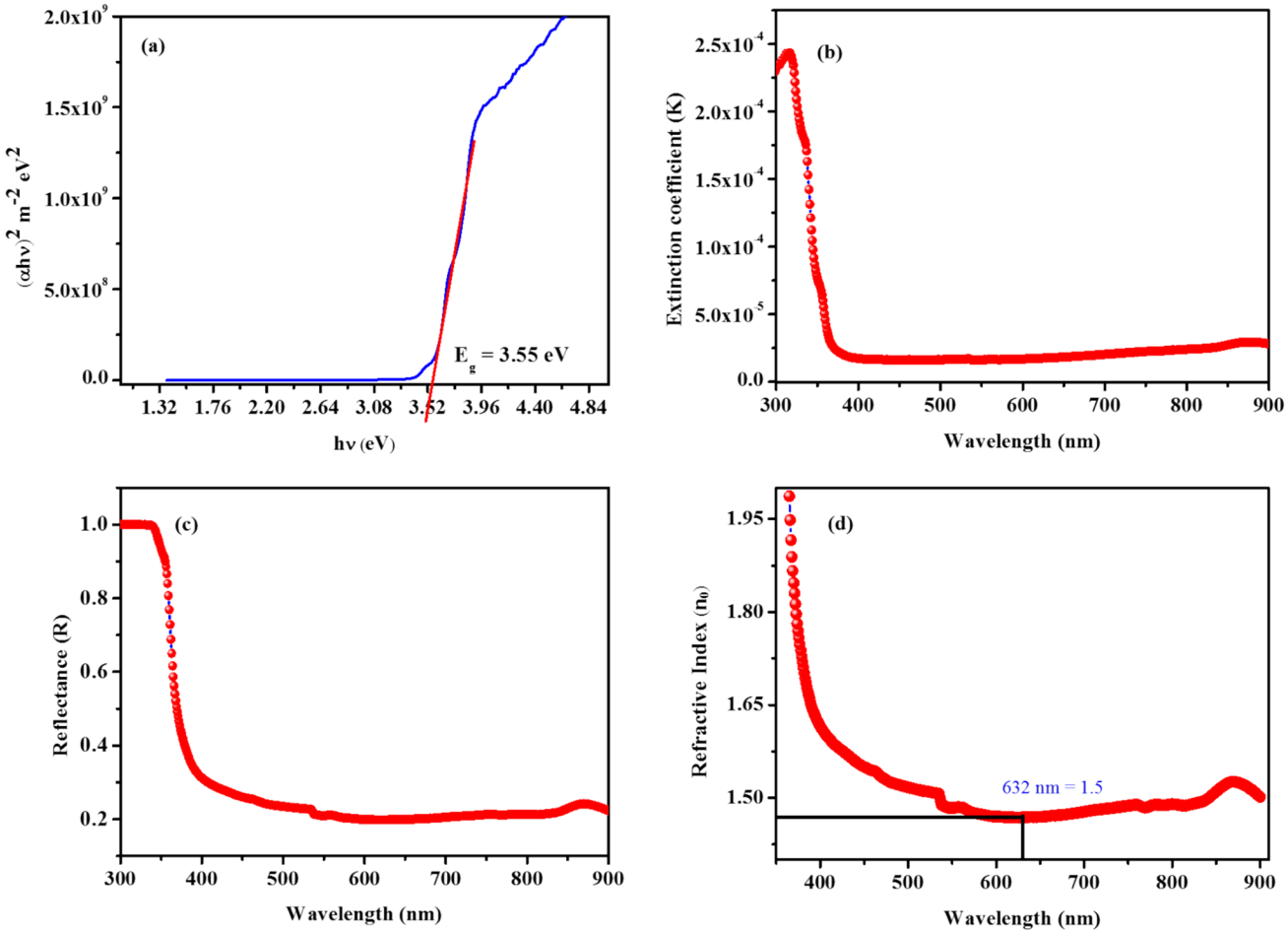

Fig. 8 **a** Optical band gap, **b** Extinction co-efficient (K), **c** Reflectance (R) and (**d**) Refractive index (n_0) of the BHSA single crystal

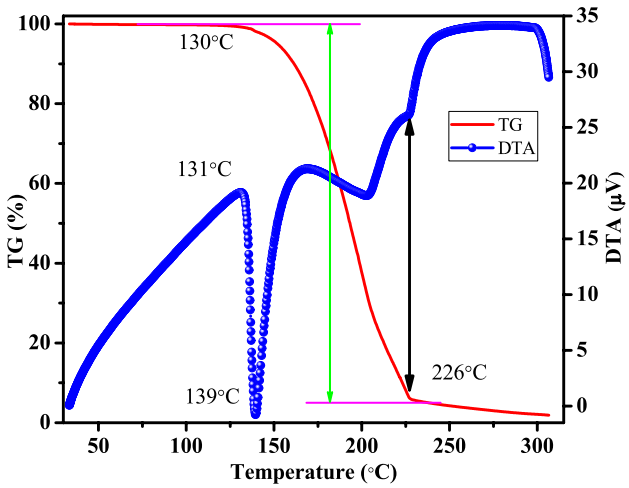

Fig. 9 TG–DTA analysis of BHSA single crystal

3.9 Z-Scan measurement

Third-order nonlinear optical properties (nonlinear absorption co-efficient (β), nonlinear refractive index (n_2) and susceptibility ($\chi^{(3)}$)) of the BHSA crystal were determined by the Z-scan method [30, 31] using He–Ne laser (632.8 nm) as input source while the sample used was of thickness 0.8 mm. The open and closed aperture spectra of BHSA crystal are shown in Fig. 13a & b, respectively. The closed aperture curve has a peak-to-valley configuration revealing that sample undergoes self-defocusing effect (negative third-order nonlinearity). The open aperture curve shows reverse saturation absorption (RSA) (i.e.) transmittance decreases as intensity increases [18, 27, 32, 33].

The third-order nonlinear optical parameters were calculated using standard expressions and the values are found to be 1.049×10^{-12} m^2/W, 2.380×10^{-06} m/W

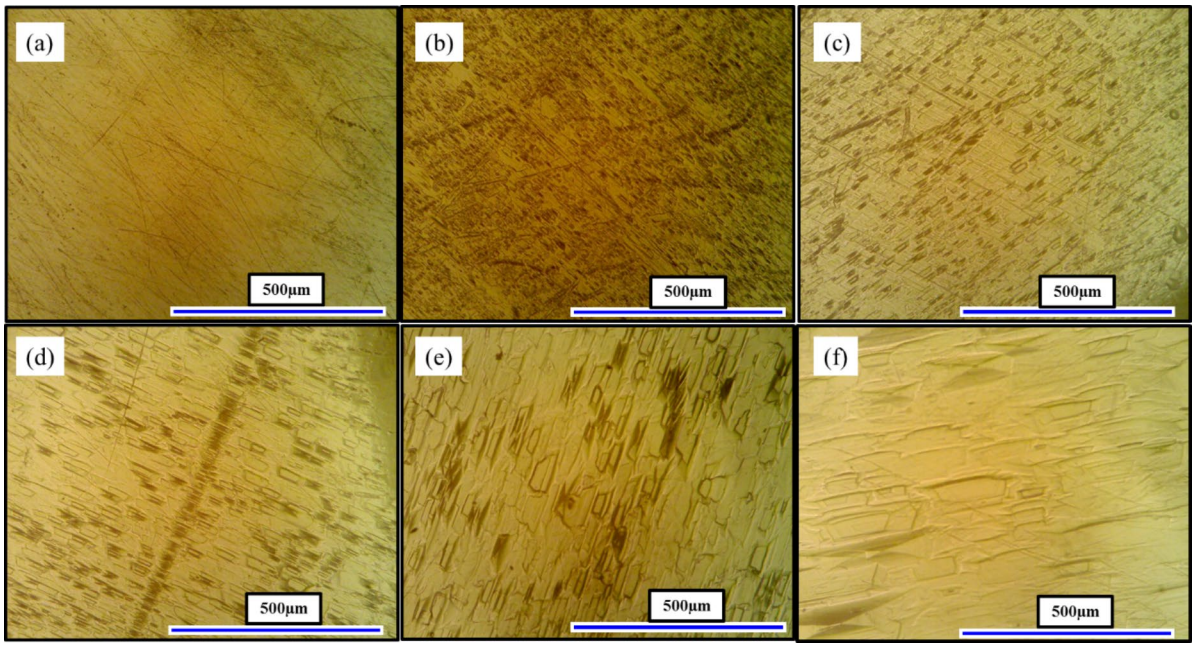

Fig. 10 **a** As grown surface, **b** 2 s, **c** 4 s, **d** 6 s, **e** 8 s and **f** 10 s etch pit pattern of BHSA single crystal

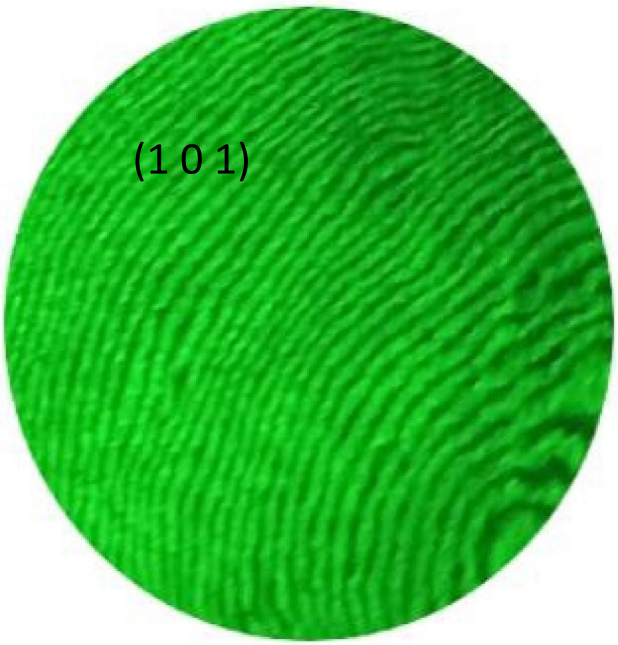

Fig. 11 Birefringence interferogram of BHSA

and 7.819×10^{-10} esu for n_2, β and $\chi^{(3)}$, respectively. The obtained results are found comparable with some of the existing salicylic acid-based crystals and is tabulated in Table 4.

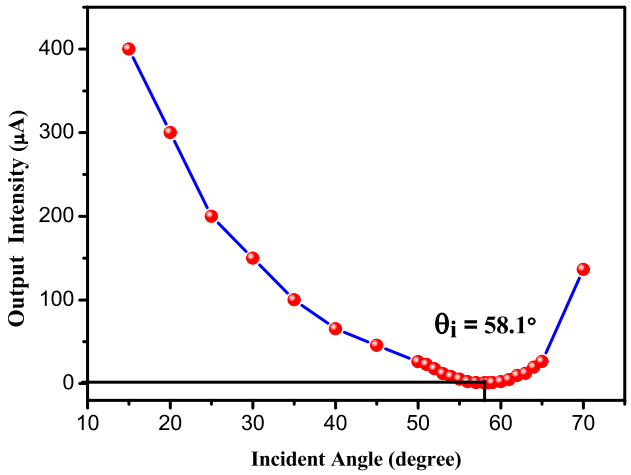

Fig. 12 Angle of rotation (Incident angle) versus Detector output

4 Conclusion

The BHSA single crystals were grown adopting slow evaporation method and it is found to crystallize in monoclinic crystal system with $P2_1/n$ space group as assessed from SC-XRD. A sharp DC obtained from the HRXRD curve confirmed the good crystalline perfection of the grown BHSA crystal. Optical transmittance revealed that the grown crystal is transparent in the entire visible region making it suitable for

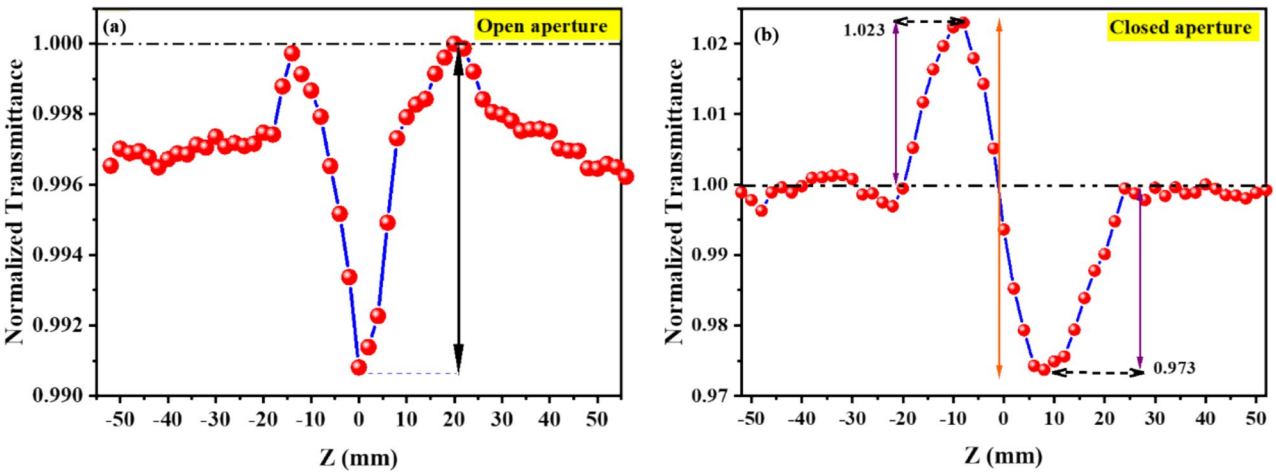

Fig. 13 **a** Open and **b** Closed aperture spectrum of BHSA crystal

Table 4 Comparison of nonlinear optical susceptibility ($\chi^{(3)}$) with salicylic acid-based crystals

Name of the crystal	$\chi^{(3)}$ esu	References
BHSA	7.819×10^{-10}	Present work
2-CPSC	2.67×10^{-6}	[34]
SA-KDOP	5.54×10^{-5}	[35]
BSL	11.3×10^{-8}	[36]

optical applications. TGA-DTA measurements reveal that the title material could be employed for practical applications in electronic components, insulation materials applicable below 131 °C. From the etching analysis the values observed are found to be low indicating the atoms/molecules are packed systematically during the growth. The birefringence study illustrates that the fringes are parallel and well-spaced, indicating that the optical homogeneity of the grown crystal is good. The third-order nonlinear optical parameters are found to be 1.049×10^{-12} m^2/W, 2.380×10^{-06} m/W and 7.819×10^{-10} esu for n_2, β and $\chi^{(3)}$, respectively, revealing that the grown BHSA crystal is a potential candidate for nonlinear optical applications.

Acknowledgements

Dr. Mohd Afzal extends his appreciation to Researchers Supporting Project number (RSPD2025R979), King Saud University, Riyadh, Saudi Arabia, for financial assistance.

Author contributions

T. Kamalesh: Conceptualization, Experimental methodology, Apparatus design and experiments, Writing—Original Draft, Apparatus design and experiments. P. Karuppasamy: Problem formulation, Design of experiment, Investigations and data analysis, Writing—Review & Editing. G. Durgababu: Data analysis. RO.MU. Jauhar, V. Kayalvizhi, M. Afzal and V. Mohan Kumar: Data analysis, Review & Editing. Muthu Senthil pandian: Review & Editing, Experiments and data analysis, Supervision and Project Administration.

Funding

There was no funding obtained.

Data Availability

Some or all data, models, or code generated or used during the study are available from the corresponding author by request (XRD, high-resolution X-ray diffraction (HRXRD), UV–Vis NIR, TG/DTA, chemical etching, birefringence interferometry, Brewster's angle method, Z-scan technique and experimental data).

Declarations

Conflict of interest The authors have not disclosed any competing interests.

References

1. Y.H. Ren, W. Li, F.Q. Zhao, J.H. Yi, B. Yan, H.X. Ma, K.Z. Xu, J.R. Song, R.Z. Hu, Crystal structure and thermal behaviors for 3,5-dinitrobenzoic acid of 3,5-diamino-1,2,4-triazole. J. Anal. Appl. Pyrolysis **102**, 89–96 (2013). https://doi.org/10.1016/j.jaap.2013.03.010
2. N. Rhimi, N. Dhahri, J. Laifi et al., Deep insights into the Cu-and W-doped Na0 5Bi0 5TiO3 solid solution: a study focusing on optical, dielectric and electrical properties. J. Mol. Str. (2023). https://doi.org/10.1016/j.molstruc.2023.136319
3. N. Rhimi, N. Dhahri, M. Khelifi, E.K. Hlil, J. Dhahri, Structural, morphological, optical and dielectric properties of sodium bismuth titanate ceramics. Inorg. Chem. Commun. **146**, 110119 (2022). https://doi.org/10.1016/j.inoche.2022.110119
4. P. Karuppasamy, T. Kamalesh, M. Senthil Pandian, P. Ramasamy, Crystal growth and physico-chemical characterization of semi-organic [C4H12N2] ZnCl4·H2O single crystal for laser applications. J. Mater. Sci.: Mater. Electron. **32**, 16467–16480 (2021). https://doi.org/10.1007/s10854-021-06203-y
5. V. Krishnakumar, M. Rajaboopathi, R. Nagalakshmi, Studies on vibrational, dielectric, mechanical and thermal properties of organic nonlinear optical co-crystal: 2,6-diaminopyridinium–4-nitrophenolate–4-nitrophenol. Phys. B **407**, 1119–1123 (2012). https://doi.org/10.1016/j.physb.2012.01.084
6. N. Rhimi, N. Dhahri, A. Dhahri, K. Dhahri, J. Dhahri, J. Juraszek, H.A. Alyousef, Cu2+ and W6+ co-doped Na0· 5Bi0· 5TiO3 solid solution: an effective approach to inhibit oxygen vacancy generation and suppress oxygen ion conduction. J. Phys. and Chem. Solids **192**, 112102 (2024). https://doi.org/10.1016/j.jpcs.2024.112102
7. L. Wang, L. Zhao, R. Xue, X. Lu, Y. Wen, Y. Yang, Construction of interesting organic supramolecular structures with synthons cooperation in the cocrystals of 1H-benzotriazole and hydroxybenzoic acids. Sci. China Chem. **55**, 2515–2522 (2012). https://doi.org/10.1007/s11426-012-4652-4
8. K.V. Patel, A. Singh, Synthesis, characterization and chelating properties of benzimidazole-salicylic acid combined molecule. J. Chem. **6**, 281–288 (2009). https://doi.org/10.1155/2009/756361
9. T. Kamalesh, P. Karuppasamy, C. Senthilkumar, M. Senthil Pandian, P. Ramasamy, S. Verma, Growth, structural, Hirshfeld surface, optical, laser damage threshold, dielectric and chemical etching analysis of 4-dimethylaminopyridinium 4-nitrophenolate 4-nitrophenol (DMAPNP) single crystal. J. Mater. Sci. Mater. Electron. **31**, 373–386 (2020). https://doi.org/10.1007/s10854-019-02536-x
10. A. Dahan, J.M. Miller, A. Hoffman, G.E. Amidon, G.L. Amidon, The solubility–permeability interplay in using cyclodextrins as pharmaceutical solubilizers: mechanistic modeling and application to progesterone. J. Pharm. Sci. **99**, 2739–2749 (2010). https://doi.org/10.1002/jps.22033
11. J.M. Miller, A. Dahan, Predicting the solubility–permeability interplay when using cyclodextrins in solubility-enabling formulations: model validation. Int. J. Pharm. **430**, 388–391 (2012). https://doi.org/10.1016/j.ijpharm.2012.03.017
12. S. Gutsche, M. Krause, H. Kranz, Strategies to overcome pH-dependent solubility of weakly basic drugs by using different types of alginates. Drug Dev. Ind. Pharm. **34**, 1277–1284 (2008). https://doi.org/10.1080/03639040802032895
13. G. Bhagavannarayana, R.V. Ananthamurthy, G.C. Budakoti, B. Kumar, K.S. Bartwal, A study of the effect of annealing on Fe-doped LiNbO3 by HRXRD, XRT and FT–IR. J. Appl. Cryst. **38**, 768–771 (2005). https://doi.org/10.1107/S0021889805023745
14. S.K. Kushwaha, N. Vijayan, G. Bhagavannarayana, Growth by SR method and characterization of bis(thiourea) zinc (II) chloride single crystals. Mater. Lett. **62**, 3931–3933 (2008). https://doi.org/10.1016/j.matlet.2008.05.027
15. J. Mohan, Organic Spectrosc.: Princ. and Appl. **2**, 487 (2004)
16. R.O.M.U. Jauhar, G. Vinitha, P. Murugakoothan, Single crystal growth of bis guanidinium hydrogen phosphate monohydrate by Sankaranarayanan-Ramasamy method and investigation of its linear and nonlinear optical properties. J. Cryst. Growth **455**, 90–93 (2016). https://doi.org/10.1016/j.jcrysgro.2016.09.012
17. P. Vivek, R.M. Jauhar, A. Suvitha, P. Era, S. Ananth, P. Murugakoothan, Habitual growth and its influence on the properties of anilinium perchlorate (AP) single crystal for nonlinear optical device applications. J. Mater. Sci.: Mater. Electron. (2018). https://doi.org/10.1007/s10854-018-8542-1
18. I. Sivagami, R.O.M.U. Jauhar, P. Era, V. Viswanathan, G. Vinitha, S. Ranjani, T. Sivanesan, Growth, structural, spectral, Hirshfeld analysis, photoluminescence, linear and third order NLO properties of a novel organic p- toluidinium succinate succinic acid single crystal. J. Cryst. Growth **580**, 126471 (2022). https://doi.org/10.1016/j.jcrysgro.2021.126471

19. J. Tauc, R. Grigorovici, A. Vancu, Optical properties and electronic structure of amorphous germanium. Phys. Stat. Sol. (b) **15**, 627–637 (1966). https://doi.org/10.1002/pssb.19660150224
20. J. Tauc, Optical properties and electronic structure of amorphous Ge and Si. Mater. Res. Bull. **3**, 37–46 (1968). https://doi.org/10.1016/0025-5408
21. A.Z. Johannes, R.K. Pingak, M. Bukit, J. Tauc, Plot Software: calculating energy gap values of organic materials based on ultraviolet-visible absorbance spectrum. IOP Conf. Ser.: Mater. Sci. Eng. **823**, 012030 (2020). https://doi.org/10.1088/1757-899X/823/1/012030
22. D.J. Stirland, G.J. Rees, A. Ritson, The relationship between etch pit density and dislocation density for (001) GaAs. J. Cryst. Growth **79**, 493–502 (1986). https://doi.org/10.1016/0022-0248(86)90482-3
23. K. Sangwal, *Etching of crystals: theory experiment and application* (Elsevier, Amsterdam, 2012)
24. K. Sangwal, M. Szurgot, Etching studies on potassium dichromate (KBC) crystals. Cryst. Res. Technol. **17**, 49–55 (1982). https://doi.org/10.1002/crat.2170170107
25. K. Sangwal, S. Veintemillas-Verdaguer, J. Torrent-Burgués, Study of growth dislocations in L-arginine phosphate monohydrate single crystals by chemical etching. J. Mater. Sci. **31**, 6299–6304 (1996). https://doi.org/10.1007/BF00354453
26. J. Gokul. Raja, M. Basheer. Ahamed, Chaudhery Mustansar Hussain, Paavai Era, Enhanced dielectric properties of PVA/PEDOT:PSS/MnO2 based composites for electronic applications. J. Mater. Sci.: Mater. Electron. **33**, 22883 (2022). https://doi.org/10.1007/s10854-022-09058-z
27. T. Kamalesh, P. Karuppasamy, M. Senthil Pandian, P. Ramasamy, S. Verma, Growth of large size triphenylphosphine oxide 4-nitrophenol (TP4N) single crystal by Sankaranarayanan-Ramasamy (SR) method for third order nonlinear optical applications. Chinese J. Phys. **76**, 68–78 (2022). https://doi.org/10.1016/j.cjph.2021.10.039
28. E.A. Tikhonov, Determ. Refract. Index of Var. Mater. Brewster Angle (2015). https://doi.org/10.48550/arXiv.1510.06850
29. E.A.B. Saleh, M.C. Teich, *Fundamentals of Photonics* (John Wiley & Sons, Hoboken, 2019)
30. M. Sheik-Bahae, A.A. Said, T.H. Wei, D.J. Hagan, E.W. Van Stryland, Sensitive measurement of optical nonlinearities using a single beam. IEEE J. Quantum Electron. **26**, 760–769 (1990). https://doi.org/10.1109/3.53394
31. M. Sheik-bahae, A.A. Said, E.W.V. Stryland, High-sensitivity, single-beam n_2 measurements. Opt. Lett. OL **14**, 955–957 (1989). https://doi.org/10.1364/OL.14.000955
32. S. Vediyappan, R. Arumugam, K. Pichan, R. Kasthuri, S.P. Muthu, R. Perumal, Crystal growth and characterization of semi-organic 2-amino-5-nitropyridinium bromide (2A5NPBr) single crystals for third-order nonlinear optical (NLO) applications. Appl. Phys. **123**, 1–15 (2017). https://doi.org/10.1007/s00339-017-1394-3
33. S. Saltiel, S. Tanev, A.D. Boardman, High-order nonlinear phase shift caused by cascaded third-order processes. Opt. Lett. **22**, 148 (1997). https://doi.org/10.1364/OL.22.000148
34. K.M. Prasad, P. Srinivasan, S.K. Barik, B.S. Lasalle, M.S. Pandian, P. Ramasamy, Studies on the synthesis, growth, and characterization of 2-cyanopyridinium salicylate single crystals for nonlinear optical applications. J. Mol. Str. **1312**, 138468 (2024). https://doi.org/10.1016/j.molstruc.2024.138468
35. M.I. Baiga, M. Anisb, S. Kalainathanc, B. Babud, G.G. Muley, Mater. Technol. **560**, 1753 (2017). https://doi.org/10.1080/10667857.2017.1321275
36. J. Jeyaram, K. Varadharajan, B. Singaram, R. Rajendhran, J. Sci.: Adv Mater. and Dev. (2017). https://doi.org/10.1016/j.jsamd.2017.09.004